Hindawi
Journal of Nanotechnology
Volume 2018, Article ID 5431290, 7 pages
https://doi.org/10.1155/2018/5431290

Research Article

Biomimetic Synthesis of Hydroxyapatite in Presence of Imidazole-4,5-dicarboxylic Acid Grafted Chitosan for Removing Chromium(VI)

Zhangxu Chen, Baorong Wu, Xiaodan Huang, Xianxue Li, and Yonglong Lin

Fujian Provincial Key Laboratory of Ecology-Toxicological Effects & Control for Emerging Contaminants, College of Environmental and Biological Engineering, Putian University, No. 1133, Xueyuan Road, Putian, Fujian 351100, China

Correspondence should be addressed to Zhangxu Chen; xuzhangchen@163.com

Received 12 January 2018; Revised 30 March 2018; Accepted 11 April 2018; Published 3 June 2018

Academic Editor: Han Zhou

In order to biomimetic synthesize hydroxyapatite similar to natural bone. Hydroxyapatite (HAP) is biomimetic synthesized in simulated body fluid (SBF) by addition of imidazole-4,5-dicarboxylic acid grafted chitosan (IDACS). The effect of molar ratio of chitosan (CS) to imidazole-4,5-dicarboxylic acid (IDA) on preparation of HAP was investigated. The structure, size, and crystal phase of the obtained hydroxyapatite were observed by Fourier transform infrared spectroscopy, X-ray powder diffraction, and scanning electron microscopy. The results show that the molar ratio of CS to IDA is 1 : 3, the temperature is 37.0°C, the aging time is 48 h, the synthesized nanorod-like hydroxyapatite with diameter 20–30 nm, and length ranging from 75 to 120 nm presents excellent phase, which disperses well and is similar to the natural bone of HAP. The obtained HAP can be used to remove chromium(VI) by the orthogonal experiments, and the results indicated that the removal rate can reach 95.66% under the optimum conditions. These results suggest that the morphology of the obtained HAP is more affected by the material ratio of chitosan to imidazole-4,5-dicarboxylic acid than its structure, and the obtained HAP can effectively remove Cr(VI), which provides a novel method for biomimetic synthesis of other biomaterials and application in the water purification.

1. Introduction

Biomimetic synthesis of biological minerals has received considerable attentions in recent years. Calcium carbonate [1–3] and hydroxyapatite [4–6] are the most abundant biological minerals, which are especially focused all over the world. Up to date, synthesis of calcium carbonate and hydroxyapatite with various strategies has been studied. Among these, ethylene glycol [7] and chitosan [8] were used as organic matrix to biomimetic synthesize calcium carbonate and hydroxyapatite. Moreover, an impersonating physiological condition, simulated body liquid (SBF), has been generally utilized as a splashing medium since it was initially arranged by Kokubo et al. [9], which has specific preferences, such as, small particle sizes and narrow size dispersion. In recent years, biomimetic synthesis of hydroxyapatite was carried out in microwave oven using 1.5 × SBF and 10 × SBF by Bindal et al. [10] and Tolga Demirtaş et al. [11]. It is worthwhile to mention that organic matrix is used as controlled template for biomimetic synthesis of calcium carbonate and hydroxyapatite in SBF solution.

Hydroxyapatite ($Ca_{10}(PO_4)_6(OH)_2$; HAP) is the one of the main biological materials, which can existed in human skeleton, animal bones, and teeth. Herein, the hydroxyapatite was formed through biomineralization and related biorelated processes, which are multifactorial, fantastic, and complex processes to commonly become a nice guide for fabrication of functional materials and keys for understanding of biophenomena [12–14].

HAP is used as a good biological material because it has particular structure and properties, such as compatibility, bioactivity, osteoconductivity, nontoxicity, and noninflammation. Therefore, it can be applied in the medical field and potentially

water purification, such as an ideal implant material, pesticides, plastic surgery, protein adsorption, and removing heavy metal. As we known, lots of researchers have devoted themselves to the medical field. Unfortunately, it still represents great challenge to apply in water purification [15]. It is well known that heavy metal pollution in groundwater or wastewater is an important environment problem due to its toxic effects and accumulation throughout the food chain and hence in the human body [16].

Removing Cr(VI) is the most important and urgent problem to be solved as human body can absorb Cr(VI) easily through the digestive, respiratory, and mucous membrane [17]. During the last decade, numbers of technologies have been adopted to remove Cr(VI) from groundwater or wastewater. However, the available publications on removing Cr(VI) by hydroxyapatite and related composites are still very limited. HAP, HAP/chitin composite, and HAP/chitosan composite were synthesized to remove Cr(VI) by Kousalya et al., and the sorption capacities of them were found to be 2720, 2845, and 3450 $mg \cdot kg^{-1}$, respectively [18]. Nanohydroxyapatite embedded gelatin composite was prepared by Gopalakannan, which was used as a biocompatible sorbent to the removal of hexavalent chromium from aqueous solution in batch mode. The adsorption capacity can reach 170 $mg \cdot g^{-1}$, and the sorption of chromium(VI) onto Nanohydroxyapatite embedded gelatin biocomposite follows Langmuir isotherm [19].

In our previous research, a series of biological materials, such as calcium carbonate and hydroxyapatite have also been successfully fabricated by using the method of biomimetic synthesis [8, 20, 21]. Encouraged by this, herein, a rational design to biomimetic synthesize hydroxyapatite for removing Cr(VI) was firstly proposed. The obtained results might significantly contribute to the practical application of biological materials as promising composites in the treatment of contaminated water.

2. Experimental Section

2.1. Materials. Imidazole-4,5-dicarboxylic acid grafted chitosan (IDACS) is synthesized according to our previous reports [20–22]. Disodium hydrogen phosphate and (Na_2HPO_4), absolute ethanol (C_2H_5OH), calcium chloride ($CaCl_2$), hydrochloric acid (HCl), and ammonia ($NH_3 \cdot H_2O$) are all of analytical reagent and are all purchased from Aladdin Reagent Co., Ltd. (China), which are used as starting materials without further purification.

2.2. Biomimetic Synthesis of Hydroxyapatite in Presence of IDACS. In this study, simulated body fluid (SBF) solution was used as solvent to replace water [23]. The hydroxyapatite crystals were obtained in pure water system [23]. To investigate the effect of IDACS on the crystallization of hydroxyapatite, different samples (S1–S5) were prepared by using IDACS as a matrix with the different molar ratio of chitosan to imidazole-4,5-dicarboxylic acid (3 : 1, 2 : 1, 1 : 1, 1 : 2, and 1 : 3), respectively. In a typical synthesis, 0.050 g of different types of IDACS was added in 25.00 mL of Na_2HPO_4 (0.06 $mol \cdot L^{-1}$), which was adjusted to pH 10.0~10.5 using ammonia or hydrochloric acid with constant stirring (Solution A). $CaCl_2$ (0.10 $mol \cdot L^{-1}$) was adjusted to pH 10.0~10.5 using ammonia or hydrochloric acid with constant stirring (Solution B). Then, Solution B was dropwise added into the above Solution A kept at a temperature of 37°C and stirred for 30 min and aged for 48 h. Finally, the obtained white precipitates were separated by centrifugation, rinsed several times with double distilled water and absolute ethanol, respectively, and then were dried in oven at 80°C until a constant weight was achieved. The as-synthesized product was denoted sample 1–5 (S1–5).

2.3. Removing Cr(VI) by Obtained Nanorod-Like Hydroxyapatite. In order to verify HAP be responsible for environmental remediation, its removing activities for chromium (VI) were investigated. The chromium sorption was studied as follows: 25 mL of chromium(VI) solution with various initial chromium(VI) concentrations were taken in a flask, and then the pH of the above solution can be adjusted by using 0.1 M HCl/NaOH solution. After adjustment, different dosage of HAP5 was added into the above solution. To explore the optimum operating condition, the L16 (4^5) orthogonal array was used in Table 1, herein, based on parallel single-factor experiment, the effect of pH value, initial concentrations of Cr(VI), dosage of HAP, and adsorption time on the removal of Cr(VI) were examined by our previous report [24].

2.4. Characterization. The sizes and morphologies of hydroxyapatite crystals were investigated by FESEM (Hitachi Model S-4800). Calibrated pellets of calcium carbonate (in proportion of 1 wt.% in KBr powder) were performed and recorded with a Fourier transform infrared spectrometer (BRUKER TENSON 27, Germany) between 4000 and 400 cm^{-1} with a resolution of 4 cm^{-1}. The X-ray diffraction (XRD) patterns were obtained on SmartLab 3 kW, X-ray diffractometer (Rigaku, Japan) using Cu Kα radiation at a scan rate of 4°C·min^{-1} was used to determine the identity of crystalline phase. The accelerating voltage and applied current were 30 kV and 40 mA, respectively.

The thermal behavior (TG) analysis of hydroxyapatite crystals were performed by using a Netzsch TG 209F3 in the temperature range of 40–1000°C with a heating rate of 10°C·min^{-1} in a dynamic atmosphere of nitrogen (60 mL·min^{-1}). The surface area and the mean pore size were determined based on the nitrogen adsorption-desorption isotherms at liquid N_2 temperature on a Micrometrics (ASAP 2020M + C) instrument. The specific surface area was determined by using the Brunauer–Emmett–Teller (BET) method. The mean pore size was estimated from the desorption branch of the nitrogen adsorption-desorption isotherms using the Barrett–Joyner–Halenda (BJH) method.

3. Results and Discussion

3.1. Influence of Molar Ratio of Chitosan/Imidazole-4,5-dicarboxylic Acid on Hydroxyapatite. Figures 1–3 present the infrared spectra, XRD patterns, and FESEM images

Table 1: Levels and factors of orthogonal experiment design.

Level	pH	Initial concentration of Cr(VI) ($mg \cdot L^{-1}$)	Dosage of HAP ($mg \cdot L^{-1}$)	Adsorption time (min)
1	3.00	25	200	90
2	5.00	50	400	120
3	7.00	100	800	150
4	9.00	200	1000	180

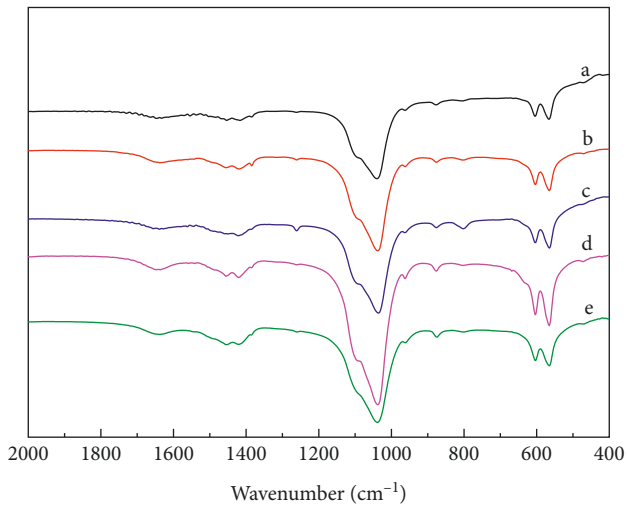

Figure 1: FT-IR spectra of HAP particles obtained by using IDACS as an organic matrix with different molar ratios of chitosan to imidazole-4,5-dicarboxylic acid. a: 3 : 1; b: 2 : 1; c: 1 : 1; d: 1 : 2; e: 1 : 3.

of the HAP crystals (S1–S5) produced with the different molar ratio of chitosan to imidazole-4,5-dicarboxylic acid (3 : 1, 2 : 1, 1 : 1, 1 : 2, and 1 : 3) at 37.0°C for aging 24 h, respectively.

As it is well known, band assignment for FT-IR of HAP was well established [25]. These absorption bands corresponding to the infrared spectra of the synthesized powders are presented in Figure 1. The presence of two bands around 565 and 604 cm^{-1} correspond to characteristic ν_4 (OPO) bending mode, and the 962 cm^{-1} band in the spectra was assigned to ν_1 (PO) symmetric stretching. 1097 and 1038 cm^{-1} were assigned to ν_3 (PO) antisymmetric stretching mode. The bands at around 1631 cm^{-1} can be indicated to the bending mode of OH^- groups. It is worth noting that the weak peaks of 1462, 1423, and 872 cm^{-1} were observed in the five spectra, 1458 and 1419 cm^{-1} are corresponding to ν_3 (CO_3^{2-}) antisymmetric stretching mode, and the band at ~872 cm^{-1} are indicated to ν_2 (CO_3^{2-}) bending mode, which is indicated that a small amount of carbonate hydroxyapatite was doped in HAP and they are similar to the main constituent of human bone [26], and it is different from HAP obtained in absence of imidazole-4,5-dicarboxylic acid grafted chitosan [23].

The same observation can also be found by XRD analysis (S1–S5 in Figures 2(a)–2(e)). The diffraction peaks occurred at $2\theta = 25.8°$, 32.1°, 33.9°, 39.5°, 46.8°, 49.7°, and 53.5°, corresponding to HAP crystal face (002), (211), (202), (310), (222), (213), and (004), respectively (JCPDS number 03-0747) [19, 22]. It indicated that HAP was all formed with different molar ratio of chitosan to imidazole-4,5-dicarboxylic acid (3 : 1, 2 : 1, 1 : 1, 1 : 2, and 1 : 3). Moreover, the intensity of X-ray diffraction patterns increased with the increasing the molar ratio of chitosan to imidazole-4,5-dicarboxylic acid, especially in the face of crystal face (211).

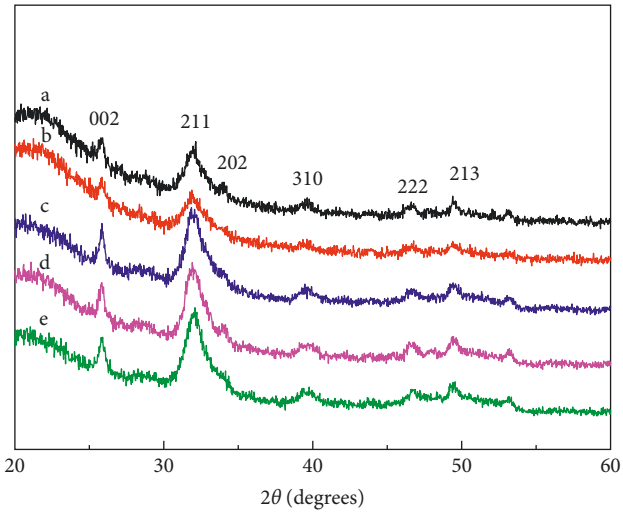

Figure 2: XRD patterns of HAP particles obtained by using IDACS as an organic matrix with different molar ratios of chitosan to imidazole-4,5-dicarboxylic acid. a: 3 : 1; b: 2 : 1; c: 1 : 1; d: 1 : 2; e: 1 : 3.

In Figure 3, FESEM images of the HAP particles obtained at various molar ratio of chitosan to imidazole-4,5-dicarboxylic acid show the morphology of HAP. When the molar ratio of chitosan to imidazole-4,5-dicarboxylic acid are 3 : 1, 2 : 1, 1 : 1, and 1 : 2, the obtained HAP presented aggregated spherical structure nanoparticles with mean diameters ~30 nm (shown in Figures 3(a)–3(d)). As the molar ratio of chitosan to imidazole-4,5-dicarboxylic acid decreases to 1 : 3, nanorod-like HAP is with the well-distributed diameters of 20–30 nm and length ranging from 75 to 120 nm. The above HAP with small particle sizes and narrow size dispersion can be biomimetic synthesized by using SBF solution. Based on the infrared spectra, XRD patterns, and FESEM images, it can be seen that the morphology of the obtained HAP is more affected by the material ratio of chitosan to imidazole-4,5-dicarboxylic acid than its structure.

The following reasons may explain these results, as the molar ratio of chitosan to imidazole-4,5-dicarboxylic acid decreases to 1 : 3, that is to say, using more imidazole-4,5-dicarboxylic acid to modify chitosan, the synthesized imidazole-4,5-dicarboxylic acid grafted chitosan (IDACS), the positive charges on its surface are surplus because of the protonation of imidazole and carboxyl groups. Because of molecular recognition and electrostatic interactions, lots of Ca^{2+} ions will aggregate on the surface of IDACS and increase surface supersaturation of Ca^{2+} ions. Meanwhile, the bonding site is offered, which would attract OH^- and CO_3^{2-}

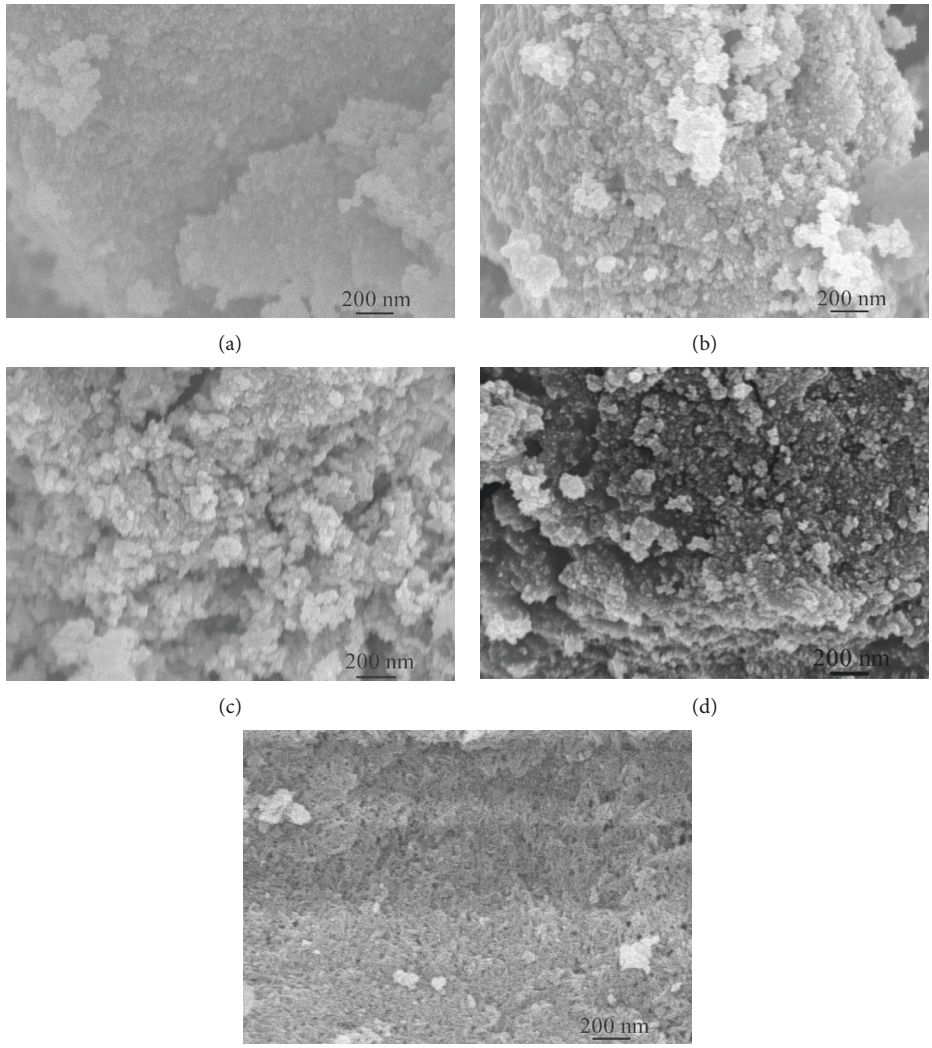

Figure 3: FESEM images of HAP particles obtained by using IDACS as an organic matrix with different molar ratios of chitosan to imidazole-4,5-dicarboxylic acid. (a) 3 : 1; (b) 2 : 1; (c) 1 : 1; (d) 1 : 2; (e) 1 : 3.

ions in the chain of IDACS and easily form the stable HAP nucleus and grow in the special crystal phase in special limited area.

3.2. Adsorption Studies. The value of the range shown in the orthogonal array indicated the influence of factors on the test index. Based on the intuitive analysis shown in Table 2, the range of pH value, initial concentration of Cr(VI), dosage of HAP, and adsorption time are 9.67, 4.76, 13.81, and 2.15, respectively. It can be shown that the pH value and dosage of HAP are the most important key factors, while the others have insignificant effects. As seen on Table 2, the results revealed that the optimum degradation conditions are as follows: the range of pH value is 3.00, initial concentration of Cr(VI) is 50 mg·L^{-1}, dosage of HAP is 1000 mg·L^{-1}, and adsorption time is 180 min. Herein, the optimum degradation condition is different from the highest removal rate (number 4) in Table 2. Therefore, the removal rate need further research under the optimum degradation condition. Verifying test results show that the obtained HAP is feasible for removal of Cr(VI) under the optimum conditions, and the degradation rate can reach 95.66%.

Based on the analysis of variance shown in Table 3, the dosage of HAP and pH value were significant influencing factors. The other factor is not significant factor. These results are agreement with the intuitive analysis.

3.3. Adsorption Mechanism. To understand the reason of removing chromium(VI) by HAP, the TG analysis, surface area, and porosity of the HAP materials are presented in Figures 4 and 5, respectively. The results obtained from the TG analysis are shown in Figure 4. As can be seen, the HAP5 obtained in SBF is stable, and the mass loss is about 2.4% of water (the weight loss below 100°C), due to the removal of adsorbed water [27], and the weight loss in the temperature range (40–900°C) investigated is ~12.1%. Furthermore, the

Table 2: Orthogonal experimental design and results.

Number	pH	Initial concentration of Cr(VI) ($mg \cdot L^{-1}$)	Dosage of HAP ($mg \cdot L^{-1}$)	Adsorption time (min)	Removal rate η (%)
1	3	25	200	90	80.85
2	3	50	400	120	86.32
3	3	100	800	150	91.73
4	3	200	1000	180	94.45
5	5	25	400	150	82.05
6	5	50	200	180	85.71
7	5	100	1000	90	89.83
8	5	200	800	120	88.36
9	7	25	800	180	88.67
10	7	50	1000	150	93.26
11	7	100	200	120	73.95
12	7	200	400	90	80.28
13	9	25	1000	120	87.45
14	9	50	800	90	83.62
15	9	100	400	180	74.37
16	9	200	200	150	69.25
Verifying test	3	50	1000	180	95.66
ADR1*	88.34	84.76	77.44	83.65	
ADR2*	86.49	87.23	80.76	84.02	
ADR3*	84.04	82.47	88.10	84.08	
ADR4*	78.67	83.09	91.25	85.80	
Range	9.67	4.76	13.81	2.15	
IF*	Secondary	Tertiary	Primary	General	

Table 3: Analysis of variance.

Source of variation	SS	df	MS	F	Significance
pH value	211.18	3	70.39	10.20	*
Initial concentration of Cr(VI)	54.30	3	18.10	2.62	
Dosage of HAP	489.07	3	163.02	23.63	*
Adsorption time	11.12	3	3.71	0.54	
Error	20.70	3	6.90	—	
Total	786.37	15	—	—	

F0.05 (3, 3) = 9.28; F0.01 (3, 3) = 29.46; *a significant influencing factors.

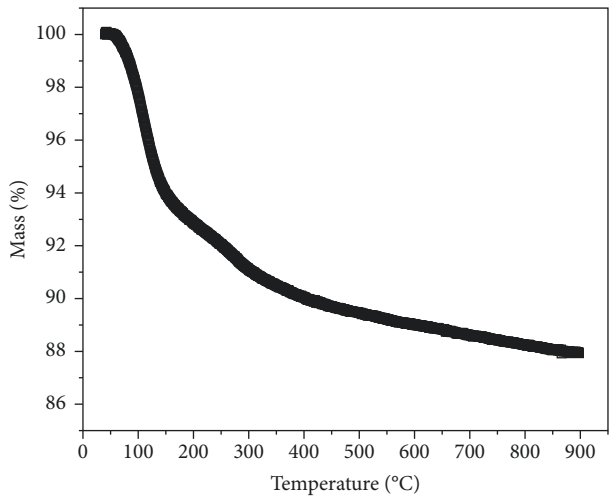

Figure 4: Thermal decomposition of HAP5.

isotherm adsorption curves for HAP5 are shown in Figure 5. In all cases, the isotherm curves have identical behaviors and can be classified as Type IV with loop H3, which is the typical characterization of mesoporous materials, suggesting the possibility of formation of slit-shape pores. Its surface area is 125.28 $m^2 \cdot g^{-1}$, the larger surface area of HAP is, the better the adsorption is, which makes HAP5 possess good adsorption capacities for chromium(VI). The pore size distribution is centered in the range of 10–20 nm, as shown in Figure 6. The mean pore size during adsorption process was determined by the BET method. This value for HAP5 is 11.59 nm, which is in agreement with the FESEM image of HAP5 in Figure 3(e).

4. Conclusion

Hydroxyapatite can be biomimetic synthesized successfully and fully characterized. The morphology of the obtained HAP is more affected by the material ratio of chitosan to imidazole-4,5-dicarboxylic acid than its structure. The formed HAP can remove chromium(VI) effectively. It can be expected that the obtained biological materials might be used for removing heavy metal in the environmental remediation or in wastewater.

Data Availability

All data generated or analysed during this study are included in this published article.

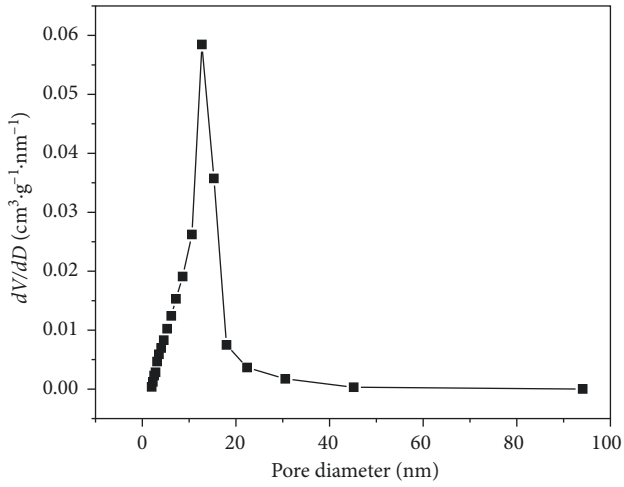

Figure 5: Pore diameter distributions of HAP5.

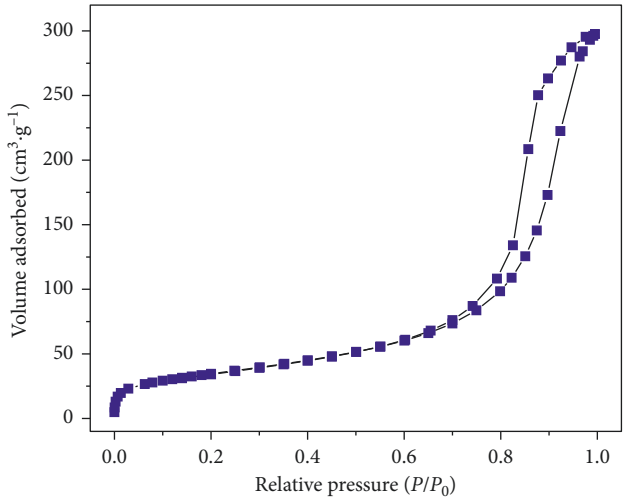

Figure 6: N_2 adsorption-desorption isotherms of HAP5.

Conflicts of Interest

The authors declare that they have no conflicts of interest.

Acknowledgments

This work was supported by the National Science Foundation of China (51478449 and 51778598), Fujian Provincial Natural Science Foundation (2015J01644, 2017J01590, and 2017J01710), Scientific Research Plan of Education Bureau of Fujian Province (JAT160431), Projects of Putian University (2015060, 2016015, and 2016065), National College Students' Innovation and Entrepreneurship Training Program Project (201711498008, 201711498006 and 201811498011), Fujian College Students' Innovation, and Entrepreneurship Training Program Project (201711498037 and 201711498034).

References

[1] J. Wu and R. J. Zeng, "Biomimetic regulation of microbially induced calcium carbonate precipitation involving immobilization of sporasarcina pasteurii by sodium alginate," *Crystal Growth and Design*, vol. 17, no. 4, pp. 1854–1862, 2017.

[2] M. A. Lopez-Heredia, A. Łapa, A. C. Mendes et al., "Bio-inspired, biomimetic, double-enzymatic mineralization of hydrogels for bone regeneration with calcium carbonate," *Materials Letters*, vol. 190, pp. 13–16, 2017.

[3] Z. Chen, B. Zheng, X. Huang et al., "Biomimetic synthesis of calcium carbonate by imidazole-1-acetic acid-grafted-chitosan," *Journal of Functional Materials*, vol. 48, no. 4, pp. 04085–04095, 2017.

[4] B. Li, L. Kan, X. Zhang et al., "Biomimetic bone-like hydroxyapatite by mineralization on supramolecular porous fiber networks," *Langmuir*, vol. 33, no. 34, pp. 8493–8502, 2017.

[5] A. Zaharia, V. Muşat, E. M. Anghel et al., "Biomimetic chitosan-hydroxyapatite hybrid biocoatings for enamel remineralization," *Ceramics International*, vol. 43, no. 14, pp. 11390–11402, 2017.

[6] F. Miculescu, A. C. Mocanu, G. E. Stan et al., "Influence of the modulated two-step synthesis of biogenic hydroxyapatite on biomimetic products' surface," *Applied Surface Science*, vol. 438, pp. 147–157, 2017.

[7] B. V. Parakhonskiy, Y. I. Svenskaya, A. M. Yashchenok et al., "Size controlled hydroxyapatite and calcium carbonate particles: Synthesis and their application as templates for SERS platform," *Colloids and Surfaces B: Biointerfaces*, vol. 118, pp. 243–248, 2014.

[8] X. Chen, M. Xin, M. Li, and Z. Chen, "Biomimetic synthesis of vaterite by *N*-succinyl-*O*-hydroxypropyl sulfonated chitosan," *Chinese Journal of Materials Research*, vol. 30, no. 1, pp. 31–37, 2016.

[9] T. Kokubo, H. Kushitani, S. Sakka, T. Kitsugi, and T. Yamamuro, "Solutions able to reproduce *in vivo* surface-structure changes in bioactive glass-ceramic A-W3," *Journal of Biomedical Materials Research*, vol. 24, no. 6, pp. 721–734, 1990.

[10] S. Türk, I. Altınsoy, G. ÇelebiEfe, M. Ipek, M. Özacar, and C. Bindal, "Microwave-assisted biomimetic synthesis of hydroxyapatite using different sources of calcium," *Materials Science and Engineering C*, vol. 76, pp. 528–535, 2017.

[11] T. Tolga Demirtaş, G. Kaynak, and M. Gümüşderelioğlu, "Bone-like hydroxyapatite precipitated from 10×SBF-like solution by microwave irradiation," *Materials Science and Engineering C*, vol. 49, pp. 713–719, 2015.

[12] Z. Wang, P. Huang, O. Jacobson et al., "Biomineralization-inspired synthesis of copper sulfide-ferritin nanocages as cancer theranostics," *ACS Nano*, vol. 10, no. 3, pp. 3453–3460, 2016.

[13] M. Okaniwa, Y. Oaki, and H. Imai, "Morphology and orientation control of organic crystals in organic media through advanced biomimetic approach," *Bulletin of the Chemical Society of Japan*, vol. 88, no. 10, pp. 1459–1465, 2015.

[14] E. Firlar, T. Perez-Gonzalez, A. Olszewska, D. Faivre, and T. Prozorov, "Following iron speciation in the early stages of magnetite magnetosome biomineralization," *Journal of Materials Research*, vol. 31, no. 5, pp. 547–555, 2016.

[15] P. Tang, Y. Zhou, and Z. Xie, "Effects of hydroxyapatite addition on heavy metal volatility during tannery sludge incineration," *Environmental Science and Pollution Research International*, vol. 20, no. 7, pp. 4405–4413, 2013.

[16] H. B. Bradl, "Adsorption of heavy metal ions on soils and soils constituents," *Journal of Colloid and Interface Science*, vol. 277, no. 1, pp. 1–18, 2004.

[17] K. Zhang, H. Li, X. Xu, and H. Yu, "Synthesis of reduced graphene oxide/NiO nanocomposites for the removal of

Cr(VI) from aqueous water by adsorption," *Microporous and Mesoporous Materials*, vol. 255, pp. 7–14, 2018.

[18] G. N. Kousalya, M. R. Gandhi, and S. Meenakshi, "Removal of toxic Cr(VI) ions from aqueous solution using nano-hydroxyapatite-based chitin and chitosan hybrid composites," *Adsorption Science and Technology*, vol. 28, no. 1, pp. 49–64, 2010.

[19] V. Gopalakannan and N. Viswanathan, "Development of nano-hydroxyapatite embedded gelatin biocomposite for effective Cr(VI) removal," *Industrial and Engineering Chemistry Research*, vol. 54, no. 50, pp. 12561–12569, 2015.

[20] Z. Chen, M. Xin, M. Li, J. Xu, X. Li, and X. Chen, "Biomimetic synthesis of coexistence of vaterite-calcite phases controlled by histidine-grafted-chitosan," *Journal of Crystal Growth*, vol. 404, pp. 107–115, 2014.

[21] Z. Chen, X. Li, and B. Zheng, "Can spherical vaterite be biomimetic synthesized by using histidine-grafted-chitosan as an organic matrix," *Journal of Inorganic and Organometallic Polymers and Materials*, vol. 27, no. 4, pp. 1014–1021, 2017.

[22] Z. Chen, M. Xin, and M. Li, "Preparation and characterization of histidine grafted chitosan porous scaffolds," *Polymer Materials Science and Engineering*, vol. 29, no. 9, pp. 152–156, 2013.

[23] Z. Chen, "Biomimetic synthesis of hydroxyapatite in presence of imidazole-1-acetic acid-grafted-chitosan scaffold," *New Chemical Materials*, vol. 45, no. 6, pp. 230–235, 2017.

[24] Z. X. Chen, B. Y. Zheng, M. L. Fu et al., "The sorption of chromium(VI) on nano-hydroxyapatite in simulated chromium(VI) wastewater," *Journal of Shandong University of Technology*, vol. 24, no. 5, pp. 20–22, 2010.

[25] Y. Deng, H. Wang, L. Zhang, Y. Li, and S. Wei, "*In situ*, synthesis and *in vitro*, biocompatibility of needle-like nano-hydroxyapatite in agar–gelatin co-hydrogel," *Materials Letters*, vol. 104, pp. 8–12, 2013.

[26] J. J. Lovón-Quintana, J. K. Rodriguez-Guerrero, and P. G. Valença, "Carbonate hydroxyapatite as a catalyst for ethanol conversion to hydrocarbon fuels," *Applied Catalysis A General*, vol. 542, pp. 136–145, 2017.

[27] D. C. Manatunga, R. M. de Silva, K. M. Nalin de Silva, N. de Silva, and E. V. A. Premalal, "Metal and polymer-mediated synthesis of porous crystalline hydroxyapatite nanocomposites for environmental remediation," *Royal Society Open Science*, vol. 5, no. 1, pp. 171557–171571, 2018.